

Position dependent microparticle charge in a spatiotemporal afterglow plasma

Citation for published version (APA):

van Huijstee, J. C. A., Blom, P., & Beckers, J. (2023). Position dependent microparticle charge in a spatiotemporal afterglow plasma. *Physics of Plasmas*, 30(3), Article 033704. <https://doi.org/10.1063/5.0139815>

Document license:

CC BY

DOI:

[10.1063/5.0139815](https://doi.org/10.1063/5.0139815)

Document status and date:

Published: 01/03/2023

Document Version:

Publisher's PDF, also known as Version of Record (includes final page, issue and volume numbers)

Please check the document version of this publication:

- A submitted manuscript is the version of the article upon submission and before peer-review. There can be important differences between the submitted version and the official published version of record. People interested in the research are advised to contact the author for the final version of the publication, or visit the DOI to the publisher's website.
- The final author version and the galley proof are versions of the publication after peer review.
- The final published version features the final layout of the paper including the volume, issue and page numbers.

[Link to publication](#)

General rights

Copyright and moral rights for the publications made accessible in the public portal are retained by the authors and/or other copyright owners and it is a condition of accessing publications that users recognise and abide by the legal requirements associated with these rights.

- Users may download and print one copy of any publication from the public portal for the purpose of private study or research.
- You may not further distribute the material or use it for any profit-making activity or commercial gain
- You may freely distribute the URL identifying the publication in the public portal.

If the publication is distributed under the terms of Article 25fa of the Dutch Copyright Act, indicated by the "Taverne" license above, please follow below link for the End User Agreement:

www.tue.nl/taverne

Take down policy

If you believe that this document breaches copyright please contact us at:

openaccess@tue.nl

providing details and we will investigate your claim.

Position dependent microparticle charge in a spatiotemporal afterglow plasma

Cite as: Phys. Plasmas **30**, 033704 (2023); <https://doi.org/10.1063/5.0139815>

Submitted: 23 December 2022 • Accepted: 22 February 2023 • Published Online: 21 March 2023

 J. C. A. van Huijstee,  P. Blom and  J. Beckers



View Online



Export Citation



CrossMark

ARTICLES YOU MAY BE INTERESTED IN

[Dust acoustic wave properties in varying discharge volumes](#)

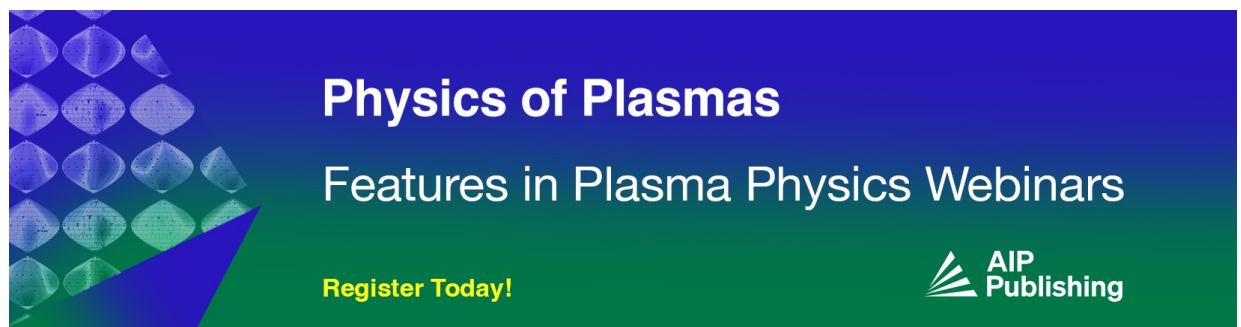
Physics of Plasmas **30**, 033703 (2023); <https://doi.org/10.1063/5.0138784>

[Three-dimensional coupling of electron cyclotron drift instability and ion-ion two stream instability](#)

Physics of Plasmas **30**, 032108 (2023); <https://doi.org/10.1063/5.0122293>


[Announcement: Physics of Plasmas Early Career Collection 2022](#)

Physics of Plasmas **30**, 030201 (2023); <https://doi.org/10.1063/5.0143348>



Physics of Plasmas
Features in Plasma Physics Webinars

Register Today!



Position dependent microparticle charge in a spatiotemporal afterglow plasma

Cite as: Phys. Plasmas **30**, 033704 (2023); doi: [10.1063/5.0139815](https://doi.org/10.1063/5.0139815)

Submitted: 23 December 2022 · Accepted: 22 February 2023 ·

Published Online: 21 March 2023



View Online



Export Citation



CrossMark

J. C. A. van Huijstee,^{1,a)}  P. Blom,²  and J. Beckers¹ 

AFFILIATIONS

¹Department of Applied Physics, Eindhoven University of Technology, P.O. Box 513, Eindhoven 5600 MB, The Netherlands

²VDL Enabling Technologies Group, P.O. Box 80038, Eindhoven 5600 JW, The Netherlands

^{a)} Author to whom correspondence should be addressed: j.c.a.v.huijstee@tue.nl

ABSTRACT

In the growing field of dusty afterglow plasma physics, the key parameter is the residual charge of dust particles. However, the particle (de-)charging process in afterglow plasmas is still far from fully understood and further development of a governing theoretical framework requires experimental data. In this work, the influence of the location of a microparticle in a spatiotemporal afterglow plasma, at the moment when the plasma was terminated, on its residual charge is investigated. It is found that the measured charge depends strongly on the local characteristic diffusion length scale of the system, while the plasma power prior to the start of the temporal afterglow phase is of much less influence. Our results contribute to an improved understanding of particle (de-)charging in afterglow plasmas and are highly relevant to the design of applications in which afterglow plasmas are present and where the charge of dust particles needs to be controlled for the sake of (nano)contamination control.

© 2023 Author(s). All article content, except where otherwise noted, is licensed under a Creative Commons Attribution (CC BY) license (<http://creativecommons.org/licenses/by/4.0/>). <https://doi.org/10.1063/5.0139815>

I. INTRODUCTION

Complex plasma physics, describing the interaction between charged nano- to micrometer sized dust particles and ionized gases (i.e., plasma), has been a growing research field over the last few decades.¹ This interest has been triggered by the great impact that its understanding has on both fundamental research areas and high-tech applications. From a fundamental viewpoint, complex plasmas offer the possibility to study microscopic processes, such as those in strongly coupled systems,^{2–4} phase transitions,⁵ and dust density waves,⁶ on macroscopic scales. Also, in other research areas, such as in astrophysics^{7,8} and aerosol science,^{9,10} the understanding of the elementary processes between charged particles and ionized media has appeared crucial. From an applied perspective, plasma can be used to synthesize and chemically modify functionalized nanomaterials¹¹ and nanoparticles.^{12–15} Furthermore, the presence of (charged) plasma-confined dust particles in nuclear fusion devices appears to have a highly negative impact on the overall process.¹⁶

The motivation for the current research is to drive the development of applications in the semiconductor industry, in which contaminating particles, embedded in plasma, play a crucially disturbing role. For instance, in extreme ultraviolet (EUV) photolithography scanners,

plasmas are inherently present,¹⁷ while particulate contaminants with sizes even down to tens of nanometers may have serious impact on the efficiency, yield, and reliability of the overall process.¹⁸ Therefore, an efficient plasma-based contamination control methodology is currently under development, which is intended to keep contamination away from sensitive surfaces inside such machines, a plasma seal particle filter.^{19,20} The concept of this plasma seal is based on the characteristic that dust particles are charged by plasma species once immersed in it. These charged dust particles can consequently be accelerated in an (externally applied) electric field and can, thus, potentially be filtered from a gas flow.

Most challenging is the fact that these two processes cannot happen simultaneously at the same location, since the plasma would then shield the electric field around the particles.²¹ Therefore, particle deflection needs to take place in a so-called afterglow plasma. Afterglow plasmas can be plasmas that decay spatially downstream the active plasma region (spatial afterglow plasmas), plasmas that decay temporally after terminating their power (temporal afterglow plasmas), or a combination of the two (spatiotemporal afterglow plasmas). To enable further development of the above-mentioned plasma seal concept, understanding of the (de-)charging of the dust particles in such environments is essential.

The evolution of the dust particle charge in afterglow plasmas has attracted much attention recently.^{22–37} However, many core concepts have remained far from understood, wherefore elementary research remains essential. Particle charging in afterglow plasmas has been investigated using both numerical simulations^{25–28} and experiments.^{29–33} From these works, it was learned that particles usually end up—in the plasma's afterglow phase—with a small negative or a positive charge. It is generally agreed upon that the transition from the ambipolar to the free diffusion regime as well as the electron density at the beginning of the afterglow phase are key parameters that determine the residual charge of the particles. Additionally, the final charge has been shown to depend strongly on externally applied electric fields in the afterglow region as well as on the gas pressure and, in the case of a high dust density, on the location of the particles.^{28–31} In Ref. 29, the microparticles even became highly positively charged when applying a DC electric field.

In this work, we present measurements of residual microparticle charges in a spatiotemporal afterglow plasma, focusing specifically on the dependence on their location in the spatial afterglow plasma at the moment the plasma power was terminated. The main difference between this work and the previously mentioned experiments is a comparatively low particle density. Moreover, the results presented here are generated in a combined spatial and temporal afterglow plasma, which, to the best of our knowledge, is not the case in any other published works apart from our previous publications.^{38,39}

The current paper is organized as follows. First, the experimental setup and the method used to measure the particle charge are introduced and explained in Secs. II and III, respectively. In Sec. IV, the results of the experiments are presented and interpreted. These results are further discussed in Sec. V. The main conclusion of the current work is highlighted in Sec. VI.

II. EXPERIMENTAL SETUP

In this section, the experimental setup that was used, of which a schematic side view is shown in Fig. 1, will be described. While this setup has been used and described in detail in several of our previous publications,^{38–43} the key aspects will be discussed here as well.

The defining characteristic of the experimental setup was a 1 m long vertical glass tube with a square $0.1 \times 0.1 \text{ m}^2$ cross section. This tube was connected to vacuum pumps, as well as to a showerhead argon inlet. During the measurements, of which the results are presented here, there was no flow present and the argon pressure was either (89.3 ± 0.6) or (29.6 ± 0.3) Pa. In each individual measurement, the pressure was constant while the plasma was on, with no fluctuations or drifts larger than the accuracy of the pressure gauge, which was 10^{-3} Pa. However, in order to reach a situation without flow, the valves to both the gas inlet and vacuum pumps had to be closed simultaneously. This was done manually, which introduced small discrepancies in the pressure between measurements. After each measurement, the setup was pumped down to the base pressure of 3×10^{-5} Pa.

Inside the glass tube, an inductively coupled plasma (ICP) was created by applying an RF voltage to a coil with five windings that was wrapped around it. The ICP was operated at low power in a capacitive mode. Measurements at the high (89.3 ± 0.6) Pa pressure were performed for three different values of RF power delivered to the plasma: 3.1, 3.9, and 5.2 W. At the lower (29.6 ± 0.3) Pa pressure, the power was decreased to 2.4 W in order to improve particle visibility.

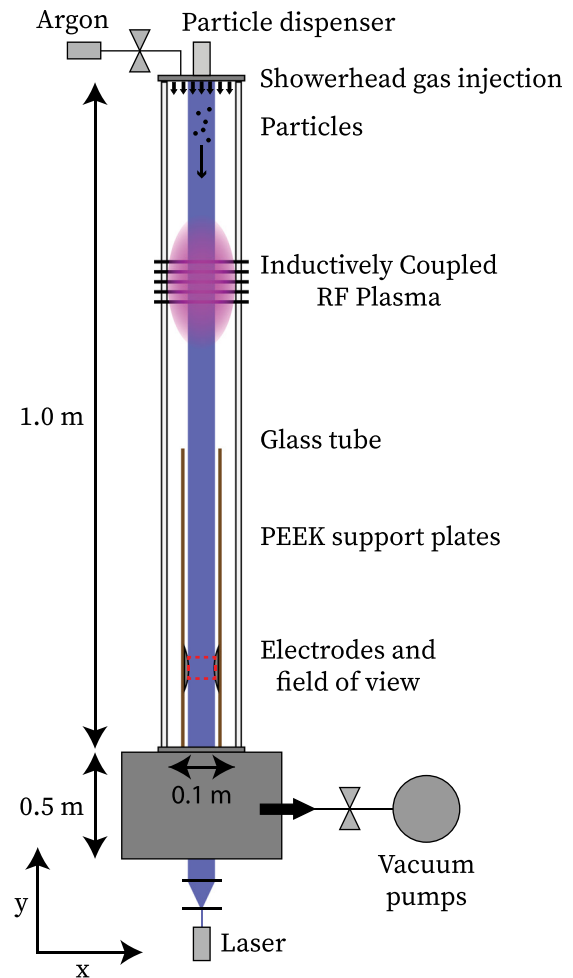


FIG. 1. Schematic side view of the experimental setup. The red rectangle represents the field of view of the high speed camera. Adapted from J. C. A. van Huijstee, P. Blom, A. T. A. Peijnenburg, and J. Beckers, *Front. Phys.* **10**, 13–16 (2022). Copyright 2022 Author(s), licensed under a Creative Commons Attribution (CC BY) license.³⁹

Furthermore, the plasma was optically characterized with an AvaSpec-3648 spectrometer. This spectrometer was able to detect light with a wavelength of (200–1100) nm with a resolution of 2.4 nm. An optical fiber connected the spectrometer to a collimation lens, which was mounted on a horizontal bar outside the glass tube at an adjustable height. This allowed for a vertically spatially resolved measurement of the plasma's light emission within the spectral range of the spectrometer.

Microparticles were injected in powder form from the top of the setup, through a slit in the showerhead. The used microparticles were made of melamine formaldehyde (MF) with a thin silver coating (to minimize undesired clustering effects) and had a producer-specified radius of $(2.48 \pm 0.09) \mu\text{m}$. After injection, the particles were illuminated by a vertically aligned blue laser sheet as they fell through the tube with a typical vertical settling velocity of (4.7 ± 0.2) or $(13.9 \pm 0.5) \text{ cm s}^{-1}$ at a pressure of (89.3 ± 0.6) or (29.6 ± 0.3) Pa, respectively.

When the particles reached the bottom of the setup, they were recorded using a Photron Mini UX100 Fastcam at a framerate of 1000 fps. The field of view of the camera was $40 \times 32 \text{ mm}^2$, imaged on 1280×1024 pixels. The camera recordings were analyzed with an in-house developed MATLAB code that reconstructed individual particle trajectories, of which both the horizontal and vertical components could be fitted perfectly with quadratic functions. From these fits, the horizontal and vertical velocities and acceleration of each particle were found.

Immediately (horizontally) outside the field of view, there were two parallel and vertically aligned Rogowski shaped electrodes to which a DC voltage could be applied.⁴⁴ These electrodes both had a diameter of 70 mm. Unless specified differently, in this work, the voltage applied to the electrodes was 10 and -10 V to the electrode immediately left and right of the field of view, respectively. The electrodes were mounted on PEEK (polyether ether ketone) plates, which extended 30 cm above the center of the electrodes in the direction of the active plasma zone.

At a certain moment in time t_p , the plasma was switched off, causing the particles to experience a temporal afterglow in addition to the spatial afterglow they were already traveling in while the plasma was on. This moment was varied from $t_p = 8$ to $t_p = 25.4 \text{ s}$ and $t_p = 4$ to $t_p = 9 \text{ s}$ after particle injection for the measurements at (89.3 ± 0.6) and $(29.6 \pm 0.3) \text{ Pa}$, respectively. The same time delay generator that triggered the plasma termination also triggered the DC voltage supplies for the electrodes 10 ms [at $(89.3 \pm 0.6) \text{ Pa}$] or 1 ms [at $(29.6 \pm 0.3) \text{ Pa}$] later. Before the trigger was sent to the voltage supplies, the electrodes were both at floating potential. This means that the external electric field was always applied after the ICP power was terminated and, therefore, did not influence the (charging of the particles in the) plasma.

All measurements were repeated at least twice to check reproducibility. Furthermore, only single spherical microparticles were included in the results analysis. Clustered particles were excluded from the data analysis based on their vertical velocity, as explained in detail in Ref. 42.

III. MEASURING METHOD

In this section, it is explained how the residual charge of microparticles is measured, as a function of their position in the setup at the moment when the plasma was terminated. To this end, it is first discussed how the location of a microparticle in the setup at the moment when the plasma was terminated is determined. This is followed by a description of how the particle charge is calculated.

As the particles are always detected in the same field of view, which is far below the active plasma zone, spatial information is acquired by varying the time at which the plasma is terminated. This is possible due to the fact that the particles have a constant (terminal) vertical velocity throughout the measurement. For each particle of which a trajectory is detected, its position at the moment when the plasma was switched off is then calculated as

$$y_0 = y - v_y(t - t_p), \quad (1)$$

where y and t are the vertical position and time of the first detection of the trajectory and t_p is the moment when the plasma is switched off. The center of the electrodes is chosen to be $y = 0$. Note that v_y is negative and t is larger than t_p , such that $y_0 > y$.

In this approach, the effect of the brief ‘‘hiccup’’ in vertical motion of the particles when the plasma is switched off is neglected. This effect appeared to be caused by sudden cooling of the former

plasma volume and is extensively described in our earlier work.³⁹ Both the duration and magnitude of this hiccup effect depend on the applied plasma power as well as on the pressure and on the initial position of the particle. Typically, for instance at a pressure of $(89.3 \pm 0.6) \text{ Pa}$ and for a plasma power of 3.1 or 3.9 W, this gives rise to an overestimation of y_0 with a magnitude of several millimeters only. For measurements at the same pressure with 5.2 W ICP power, this can increase to more than a centimeter. At $(29.6 \pm 0.3) \text{ Pa}$, the overestimation is less (approximately 1 mm).

Furthermore, measuring the charge of the microparticles as a function of their position y_0 in the spatial afterglow at the moment when the plasma power was terminated requires the particles to remain at roughly the same vertical position during the full temporal decay of the (spatial afterglow) plasma. In other words, it is assumed that the position of the particle when its charge becomes frozen is equal to y_0 . This assumption holds when the changes in the plasma that a particle experiences due to the temporal decay are much faster than those due to its motion in space. The timescale of the temporal afterglow in the relevant conditions is typically in the order of milliseconds, after which the particles’ charge is frozen (see Sec. IV).²⁵ During 1 ms, particles with a vertical velocity of $-4.7 \times 10^{-2} \text{ m s}^{-1}$ would fall $4.7 \times 10^{-5} \text{ m}$, which is only one order of magnitude larger than the size of the particles themselves and much smaller than the typical dimensions of the plasma. This is also the case at lower pressure, at which the effect of the increased velocity of the particles ($\propto \frac{1}{p}$) is negated by the decreased plasma density decay timescale ($\propto p$). Therefore, the particles can safely be assumed stationary during the full decay of the plasma.

In addition, it is assumed that the particle charge does not change between the moment the plasma has fully decayed and the moment of charge measurement downstream.

The charge of each microparticle is calculated by analyzing its trajectory, which is influenced by the electric field between the two vertically parallel electrodes at the bottom of the setup, and solving the horizontal force balance. After the plasma is terminated and a DC voltage is supplied to the electrodes, the microparticles experience a constant horizontal electric field. Since the plasma power is switched off before the particles are recorded, a constant particle charge and no plasma induced forces are expected. These assumptions are verified with measurements (included in the [supplementary material](#)), where it is shown that the measured charge is independent of the applied electric field and that the particles have no horizontal acceleration in the field of view. This results in a simple balance of the forces acting on the particles in the horizontal direction as follows:

$$F_{E,x} + F_{d,x} = m_p a_x, \quad (2)$$

where the electrostatic force is given by

$$F_{E,x} = Q_p E_x, \quad (3)$$

and the Epstein neutral drag force is given by⁴⁵

$$F_{d,x} = -\frac{4\pi}{3} \delta v_{Th} \rho_g r_p^2 v_x. \quad (4)$$

Here, m_p is the particle mass, r_p is the particle radius, and δ is a constant with a value of 1–1.442 specifying the physical nature of micro-scope atom–particle interactions. Furthermore, v_{Th} and ρ_g are the

thermal velocity and mass density of the argon gas, respectively; v_x and a_x are the horizontal velocity and acceleration of the microparticle; and E_x is the magnitude of the externally applied electric field in the horizontal direction.

The force balance of Eq. (2) can be rewritten to solve for the particle charge

$$Q_p = \frac{1}{E_x} \left(m_p a_x + \frac{4\pi}{3} \delta v_{\text{Th}} \rho_g r_p^2 v_x \right). \quad (5)$$

The velocity and acceleration are measured for each individual particle, as described earlier. Due to the surface roughness and thermal non-conductivity of the coating layer, the argon-microparticle collisions are expected to be diffuse, meaning $\delta = 1.442$.⁴⁵ The thermal velocity and mass density of the argon gas, as well as the magnitude of the horizontal electric field E_x , are known constants in the experiments. Furthermore, the radius (and mass) of each individual particle is determined from its vertical velocity v_y as follows:

$$r_p = \delta v_{\text{Th}} \frac{\rho_g v_y}{\rho_p g}, \quad (6)$$

as was done previously in Ref. 42. It is assumed that all particles included in the analysis are spherical and have the same average mass density of $\rho_p = 1.61 \times 10^3 \text{ kg/m}^3$, with their vertical velocity determined by a balance between gravity and the neutral drag force. Note that the direction of the gravitational acceleration is defined as the negative vertical direction, so $g = -9.81 \text{ m/s}^2$ and v_y is also negative.

IV. RESULTS AND INTERPRETATION

The charges of the microparticles, obtained as a function of their position y_0 at the moment when the plasma was terminated, are plotted in Fig. 2 for three different plasma powers. The data are sorted into bins of y_0 with a width of 5 mm. Due to the discrete values of t_p that are used, particles are not detected for all values of y_0 . Each datapoint in the figure represents the average of all measured values in that bin, with the errorbars indicating the standard deviation. This means that the errorbars in this figure do not represent actual errors in the data. The error in each detection is much smaller than the standard deviation of the ensemble, which arises from the stochastic nature of the charging process and spread in the radii of the particles.

Figure 2 can be divided into three different regions, corresponding to distinct physical regions in the setup. We will number the three regions starting from the highest value of y_0 , which is closest to the point of particle injection.

- **Region I** ($y > 0.3 \text{ m}$): the region where the ICP is created. Particles from this region have a residual charge of approximately zero.
- **Region II** ($0.06 \text{ m} < y < 0.3 \text{ m}$): the region between the PEEK plates. Here, the negative particle charge is constant and several hundreds of electron charges in magnitude.
- **Region III** ($y < 0.06 \text{ m}$): the region between the electrodes. Particles from this region are even more negatively charged. The negative particle charge reaches a maximum for y_0 just above zero and decreases again for lower positions.

There are two main takeaways from Fig. 2: first, the charge is mostly independent of the ICP power and second, there is a clear

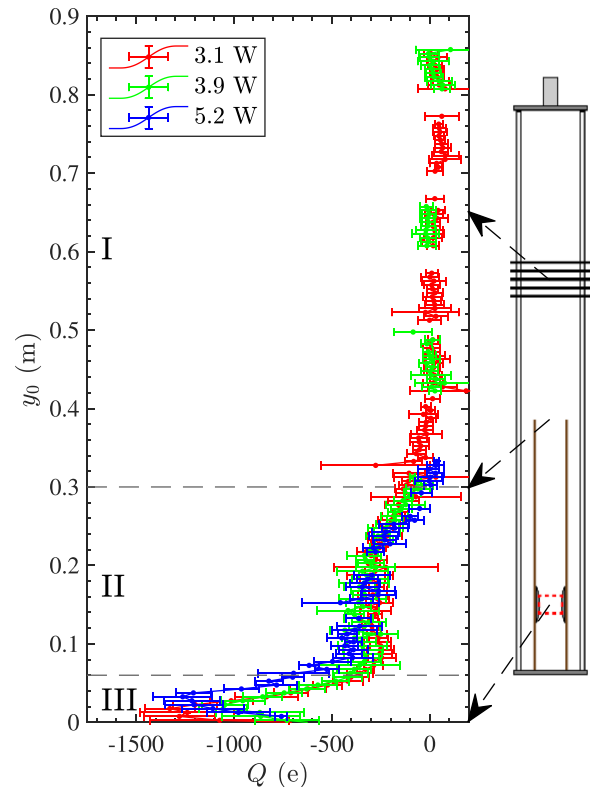


FIG. 2. The average charge of the detected microparticles as a function of their position when the plasma was switched off, for three different plasma powers at an argon pressure of $(89.3 \pm 0.6) \text{ Pa}$. The center of the electrodes is set as $y_0 = 0$ and the errorbars represent the standard deviation.

correlation between the particle charge and the location of the particle in the setup. Measurements are performed for 3.1, 3.9, and 5.2 W plasma power, of which the results are shown in red, green, and blue, respectively. It is clear that there are no significant differences between these three cases in regions I and II. In region III, the particle charge seems to reach its maximum negative value at higher y_0 for increasing values of ICP power. However, this is most probably due to the larger overestimation of y_0 (see Sec. III) and not an actual charging effect.

The fact that changing the plasma power does not influence the measured particle charge significantly indicates that this charge is dominantly determined by the (de)-charging process in the temporal afterglow rather than that in the spatial afterglow. Since differences in power should cause variations in the spatial profile of the electron density and temperature, the initial charge of the particles in the spatial afterglow plasma would be expected to change with the plasma power. However, the measured particle charge shows no significant dependence on power. Therefore, the (de)-charging in the temporal afterglow appears to be the dominant process that determines the residual particle charge.

From a theoretical point of view, the particle charging process in a temporal afterglow plasma can be characterized using three time-scales:^{23–25,36} the timescales for electron density decay (τ_D), electron cooling (τ_T), and particle (de)-charging (τ_C). Particles will have the

expected equilibrium charge in their environment as long as their (de)-charging happens faster than the variation in their environment, or $\tau_C \leq (\tau_D \text{ and } \tau_T)$. Initially in the temporal afterglow, this will be the case. The negative charge of the particles decreases due to a decreasing electron current to the particle surface as the electron temperature cools down. At a certain moment in time, the charging timescale will become (much) larger than the other two timescales and the particle charge no longer changes. This (frozen) residual charge is what we measure in our experiments.

The charging timescale is a quite complicated parameter, since it depends on the local electron temperature as well as on the electron and ion densities and the existing charge of the microparticle. However, at the pressure that we are interested in, electron cooling happens at a timescale in the order of microseconds.²⁵ This is several orders of magnitude faster than the decay of the plasma density, which is in the millisecond range [using Eq. (8), as will be explained later, $\tau_D \simeq 4.2 \text{ ms}$ for $p = 89.3 \text{ Pa}$, $T_e = 1 \text{ eV}$, and $\Lambda = 22.5 \text{ mm}$].

We, therefore, assume that the variations in the residual charge of the particles for different values of y_0 depend only on the decay of the plasma densities and not on the electron temperature cooling. A fast decay of densities then results in a high negative charge, while a slower density decay gives the particles the chance to discharge further, possibly even reaching a positive charge. Since three body recombination is negligible in the system at low pressure, loss of plasma species happens predominantly due to diffusion to the walls. Ambipolar density decay in a temporal afterglow plasma can be described as²⁵

$$\frac{d\tilde{n}}{dt} = -\frac{\tilde{n}}{\tau_D}, \tag{7}$$

where $\tilde{n} = \frac{n_{ie}}{n_0}$ is the ratio between the time dependent and initial ion or electron densities and the ambipolar diffusion timescale,^{24,25,46}

$$\frac{1}{\tau_D} \simeq \frac{\lambda_{mfp,i} v_{Th,i}}{3\Lambda^2} (1 + \tilde{T}_e). \tag{8}$$

Here, $\lambda_{mfp,i}$ and $v_{Th,i}$ are the mean free path and thermal velocity of the ions, respectively. Furthermore, Λ is the characteristic diffusion length, related to the size of the plasma container, and $\tilde{T}_e = \frac{T_e}{T_i}$ is the ratio of the electron and ion temperatures, which quickly becomes equal to 1 during the afterglow phase. Note that Eq. (8) is only valid for sufficiently low microparticle densities, as is the case in our experiments. For situations with a high dust density, an additional term accounting for electron and ion losses at the particles' surfaces should be included, which would decrease the characteristic decay time.

Equation (8) states that the ambipolar diffusion timescale scales with the characteristic diffusion length Λ as Λ^{-2} . In a tube with a rectangular cross section with sides of length A and B , the characteristic diffusion length of the system is defined as^{47,48}

$$\frac{1}{\Lambda^2} = \left(\frac{\pi}{A}\right)^2 + \left(\frac{\pi}{B}\right)^2, \tag{9}$$

which reduces to

$$\Lambda = \frac{A}{\sqrt{2}\pi} \tag{10}$$

in a tube with a square cross section of $A \times A$.

The main physical characteristic separating the three regions of the experimental setup (as also indicated in Fig. 2) is the local diffusion length. In region I, the plasma volume is bounded by the walls of the glass tube, which has a square cross section with length $A = 100 \text{ mm}$. Using Eq. (10), this equates to $\Lambda = 22.5 \text{ mm}$. Region II includes the two PEEK plates, which decrease the size of the plasma volume in one dimension, resulting in $\Lambda = 16.4 \text{ mm}$ (for $B = 60 \text{ mm}$). Between the electrodes, in region III, the diffusion length is even smaller. Taking B equal to the distance between the centers of the electrodes (40 mm) gives $\Lambda = 11.8 \text{ mm}$. However, due to the curved shape of the electrodes, the diffusion length is not constant in this region.

So far we have shown that the residual particle charge is expected to depend on the characteristic diffusion length of the system and have seen that the measured values are, indeed, different in the three regions of y_0 in the experimental setup with different diffusion lengths. In region I, the diffusion length is the largest, corresponding to the largest diffusion timescale. Figure 2 shows that the particles have, indeed, had sufficient time to discharge completely if they were in that region when the plasma power was terminated. On the other hand, in region II, the diffusion length is shorter and the residual particle charge is measured to be negative, because the particles apparently did not have enough time to fully discharge. Region III shows the effect of the diffusion length best, as the measured charge of the particles from this region is, indeed, even more negative and approximately follows the shape of the electrodes.

In conclusion, the results suggest that the characteristic diffusion length and, therefore, the geometry of the vessel is key for the charge of the particles after experiencing the spatiotemporal afterglow plasma. Meanwhile, the initial plasma conditions are much less relevant.

V. DISCUSSION AND VERIFICATIONS

To support the conclusion drawn from Sec. IV, two more verifications should be done. First, the plasma density should be sufficiently high throughout the tube, so that the initial charge in the spatial afterglow plasma remains (highly) negative. Second, as the diffusion length only depends on the geometry of the vessel, varying the neutral gas pressure should result in similar trends in the measured charge. It will be shown in Secs. VA and VB that these two considerations, indeed, match expectations and support our findings.

A. Plasma density

For the final charge to be dominantly determined by the diffusion timescale, it is required that the microparticles retain a (high) negative charge throughout the spatial afterglow plasma. This implies that, when the ICP power is supplied, the entire volume should be in the ambipolar diffusion regime, where the ion and electron densities are approximately equal. Ambipolar diffusion is expected to break down when the Debye length λ_D becomes similar to the characteristic diffusion lengthscale.^{23,26,48,49} In practice, there is a gradual transition to the free diffusion regime. As an estimate, $\lambda_D = 10^{-1}\Lambda$ is taken as a critical value for transition to the free diffusion regime, resulting in a critical electron density $\sim 1 \times 10^{12} \text{ m}^{-3}$ between the electrodes in our setup.

The plasma, at a pressure of $(89.3 \pm 0.6) \text{ Pa}$ and ICP power of 3.3 W , is characterized with a spectrometer and the spectrum intensity is used as an indication for the plasma density. To this end, the total intensity of the emitted light in the range (810–814) nm is measured at

different positions y . This wavelength range corresponds to the location of the most prominent peak in the measured spectrum, which is due to two separate transitions of 4p argon states to metastable 4s states at 810.37 and 811.53 nm. Due to the limited resolution of the used spectrometer, it is not possible to distinguish between the two transitions. However, it is reasonable to take the measured intensity as a qualitative measure of the electron density, since both 4p states are predominantly populated by electron impact reactions with the ground state and have a lifetime in the order of nanoseconds.⁵⁰

The intensity as a function of position y is plotted in Fig. 3. This intensity is equal to the total number of counts per second in the range of 810–814 nm. Here, the average of ten measurements was taken for each datapoint and the average number of counts and standard deviation therein were calculated for all 12 pixels in the selected range. Only pixels where the plasma emission is significant were taken into account in the total intensity. This means that the intensity as shown in the figure is equal to the sum of all pixels for which the average intensity is larger than the standard deviation. For the measurements at $y = -0.03$ and 0.02 m, plotted as open circles, there are no such pixels and the same pixels as for the measurement at $y = 0.07$ m are taken. These two datapoints are indistinguishable from noise.

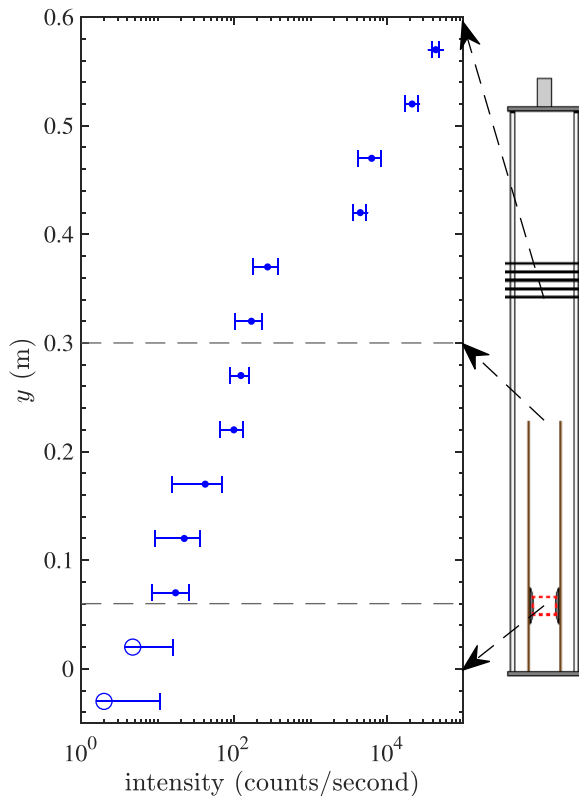


FIG. 3. Total plasma intensity in the range of 810–814 nm as a function of the position y in the tube for an ICP power of 3.3 W and at a pressure of (89.3 ± 0.6) Pa. Each datapoint represents the average of 10 measurements, with the standard deviation as an errorbar. The two points plotted as open circles have a standard deviation extending below zero and are, therefore, not distinguishable from noise.

Clearly, the plasma extends far below the ICP coil, which is positioned at $y = (0.6 - 0.7)$ m, just outside the axis limits of Fig. 3. The two datapoints at the lowest y values fall below the detection limit of the spectrometer. The limiting factor, here, is the spectrometer’s sensitivity. This does not necessarily mean that there is no more plasma present at these positions, but only that the spectrometer cannot measure it. Assuming that the measured intensity scales linearly with the electron density⁵⁰ and without taking into account the drop in intensity due to the decreasing electron temperature, Fig. 3 indicates that the electron density drops at most a factor 10^4 over the length of the tube. Taking $n_e = 10^{16} \text{ m}^{-3}$ as a typical minimum electron density value for low power ICPs at the bottom of the coil,²¹ the electron density near the electrodes would remain at least 10^{12} m^{-3} . Since the decrease in electron temperature is neglected in this approach, which is responsible for a significant part of the drop in measured intensity, the electron density is expected to still be above the calculated threshold of $\sim 1 \times 10^{12} \text{ m}^{-3}$ for the transition to the free diffusion regime. This suggests that the particles could, indeed, remain negatively charged throughout the spatial afterglow plasma under the current conditions.

B. Verification at lower pressure

The main conclusion from Sec. IV is that the residual particle charge depends strongly on the characteristic diffusion length Λ of the system. This is based on the fact that the measured particle charge in Fig. 2 can clearly be divided into three different regions, which correspond to regions in the setup where the diffusion length differs. Since a critical reader might suspect this to be a mere coincidence, additional measurements are performed with changed plasma parameters. Considering Λ is a function of only the geometry of the setup, the same three regions should still be visible when the plasma parameters are changed. A parameter that is known to significantly influence the (residual) charge of particles in a(n) afterglow plasma is the neutral gas pressure.^{28,51} This also follows directly from Eq. (8), where the ion mean free path $\lambda_{\text{mfp},i}$ scales inversely with the pressure. Therefore, in order to verify the conclusion, the measurements of which the results are shown in Sec. IV are repeated at a lower pressure.

In Fig. 4, the charge of particles as a function of their position y_0 at the moment when the plasma was switched off, is plotted in blue for measurements with a neutral gas pressure of (29.6 ± 0.3) Pa. This is compared to the measurements at higher pressure, which is the same data as shown in red in Fig. 2. Absolute values of the charge are hard to compare, since the plasma (and, therefore, the particle charging process) changes significantly when the pressure and power are decreased. Nevertheless, trends in the data can be compared.

At low pressure, the trend in particle charge is similar to that at high pressure: the same three regions are visible. If the particle was in region I when the plasma power was terminated, the measured residual particle charge is still approximately zero. Particles from region II are again measured to have a negative charge. The absolute value of the charge of these particles is significantly higher compared to the (89.3 ± 0.6) Pa case. This matches expectations, if the charge is determined dominantly by discharging in the temporal afterglow with time-scale τ_D [Eq. (8)]. In region III, the particle charge behaves differently from expectations. It first becomes slightly less negative, before going back to the value that is measured in region II. Possibly the assumption that the charge remains highly negative no longer holds in this

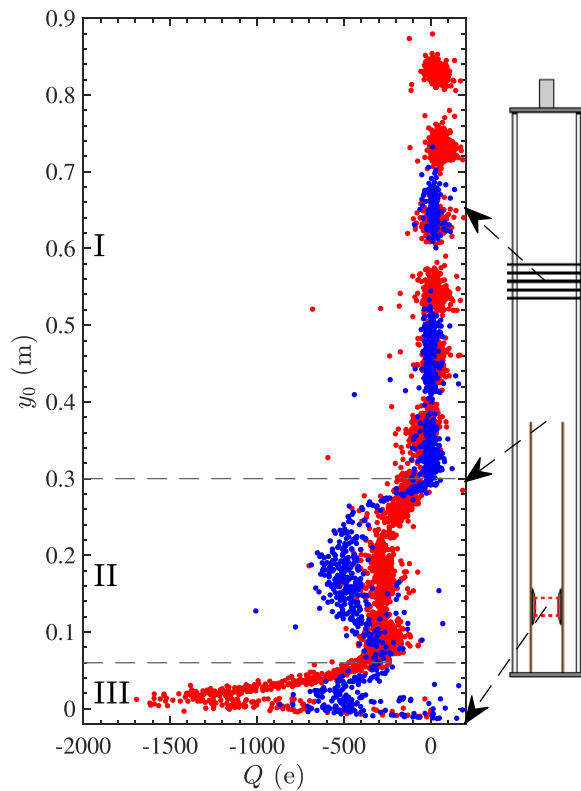


FIG. 4. The charge of detected microparticles as a function of their position when the plasma is switched off for measurements with a pressure of (29.6 ± 0.3) Pa and a plasma power of 2.4 W in blue, compared with the (89.3 ± 0.6) Pa data at 3.1 W plasma power in red. The latter is the same data as plotted in red in Fig. 2.

region at lower pressure (or in other words, the decharging in the spatial afterglow significantly influences the results here, which it did not previously). This is plausible, since both the pressure and plasma power have been decreased. Therefore, the electron density is expected to be lower and might have fallen below the critical value for the transition to the free diffusion regime.

However, the fact that the same three regions are visible in the results for the same values of y_0 supports the insight that the measured trends are, indeed, determined by the characteristic diffusion length, or in other words, the geometry of the setup.

VI. CONCLUSION

In this work, it is found that the residual charge of microparticles in a spatiotemporal afterglow plasma depends strongly on the local characteristic diffusion length of the system. Meanwhile, the plasma power is of much less influence. These results are acquired by measuring the residual charge of microparticles after they experience a spatiotemporal afterglow plasma. In specific, the influence of the location of the particle, at the moment when the plasma was terminated, on its residual charge is investigated. If the particles were already in the measurement volume, where the characteristic diffusion length is minimum, at the moment at which the plasma was switched off, high negative charges of up to 1500e are measured. However, if the particles

were in a region with a larger characteristic diffusion length, further away from the detection plane, at the moment at which the plasma was switched off, the measured particle charge approaches zero. This means that the particles have been fully discharged during their travel toward the detection plane.

From a fundamental point of view, our results contribute to expanding the understanding of particle (de)-charging in afterglow plasmas. Of specific interest in such afterglow plasma systems is the peculiar transition from the ambipolar diffusion regime to the free diffusion regime.^{23,26} The current experiments provide an ideal test case for verification, validation, and benchmarking of numerical and analytical modeling efforts in the field. Additionally, our findings are highly relevant for the design of applications where there are afterglow plasmas present and the charge of particles should be controlled. These applications include state-of-the-art plasma-enabled nanocontamination control strategies^{19,20} and plasma seals for robotic feed-throughs in ultraclean vacuum systems.

SUPPLEMENTARY MATERIAL

See the [supplementary material](#) for the measurements to verify the assumptions that, while their charge is measured, the microparticles have a constant charge and experience no plasma induced forces.

ACKNOWLEDGMENTS

This study received financial support from VDL Enabling Technologies Group. The authors are grateful to Pieter Sanders, Ab Schrader, and Jürgen Kohlhepp for their technical support.

AUTHOR DECLARATIONS

Conflict of Interest

The authors have no conflicts to disclose.

Author Contributions

Judith van Huijstee: Data curation (lead); Formal analysis (lead); Investigation (lead); Methodology (lead); Software (lead); Validation (lead); Visualization (lead); Writing – original draft (lead); Writing – review & editing (equal). **Paul Blom:** Conceptualization (equal); Funding acquisition (equal); Project administration (equal); Writing – review & editing (equal). **Job Beckers:** Conceptualization (equal); Formal analysis (supporting); Funding acquisition (equal); Project administration (equal); Resources (equal); Supervision (lead); Writing – review & editing (equal).

DATA AVAILABILITY

The data that support the findings of this study are available from the corresponding author upon reasonable request.

REFERENCES

- ¹P. K. Shukla and A. A. Mamun, *Introduction to Dusty Plasma Physics* (Institute of Physics Publishing, 2002).
- ²G. E. Morfill, A. V. Ivlev, S. A. Khrapak, B. A. Klumov, M. Rubin-Zuzic, U. Konopka, and H. M. Thomas, “Ten years of plasma crystals - From ICPIG (Bochum) to ICPIG (Greifswald),” *Contrib. Plasma Phys.* **44**, 450–457 (2004).

- ³G. E. Morfill, A. V. Ivlev, M. Rubin-Zuzic, C. A. Knapek, R. Pompl, T. Antonova, and H. M. Thomas, "Complex plasmas - New discoveries in strong coupling physics," *Appl. Phys. B* **89**, 527–534 (2007).
- ⁴H. M. Thomas, M. Schwabe, M. Y. Pustyl'nik, C. A. Knapek, V. I. Molotkov, A. M. Lipaev, O. F. Petrov, V. E. Fortov, and S. A. Khrapak, "Complex plasma research on the International Space Station," *Plasma Phys. Controlled Fusion* **61**, 014004 (2019).
- ⁵B. Smith, T. Hyde, L. Matthews, J. Reay, M. Cook, and J. Schmoke, "Phase transitions in a dusty plasma with two distinct particle sizes," *Adv. Space Res.* **41**, 1510–1513 (2008).
- ⁶R. L. Merlino, "25 years of dust acoustic waves," *J. Plasma Phys.* **80**, 773–786 (2014).
- ⁷L. S. Matthews, V. Land, and T. W. Hyde, "Charging and coagulation of dust in protoplanetary plasma environments," *Astrophys. J.* **744**, 8 (2012).
- ⁸F. Verheest, "Waves and instabilities in dusty space plasmas," *Space Sci. Rev.* **77**, 267–302 (1996).
- ⁹A. Mizuno, "Industrial applications of atmospheric non-thermal plasma in environmental remediation," *Plasma Phys. Controlled Fusion* **49**, A1 (2007).
- ¹⁰R. Gopalakrishnan, P. H. McMurry, and C. J. Hogan, "The bipolar diffusion charging of nanoparticles: A review and development of approaches for non-spherical particles," *Aerosol Sci. Technol.* **49**, 1181–1194 (2015).
- ¹¹N. K. Kaushik, N. Kaushik, N. N. Linh, B. Ghimire, A. Pengkit, J. Sornsakdanuphap, S. J. Lee, and E. H. Choi, "Plasma and nanomaterials: Fabrication and biomedical applications," *Nanomaterials* **9**, 98 (2019).
- ¹²F. Zhu, J. Zhang, Z. Yang, Y. Guo, H. Li, and Y. Zhang, "The dispersion study of TiO₂ nanoparticles surface modified through plasma polymerization," *Physica E* **27**, 457–461 (2005).
- ¹³N. Rao, S. Girshick, J. Heberlein, P. McMurry, S. Jones, D. Hansen, and B. Micheel, "Nanoparticle formation using a plasma expansion process," *Plasma Chem. Plasma Process.* **15**, 581–606 (1995).
- ¹⁴J. Phillips, C. C. Luhrs, and M. Richard, "Review: Engineering particles using the aerosol-through-plasma method," *IEEE Trans. Plasma Sci.* **37**, 726–739 (2009).
- ¹⁵T. J. M. Donders, T. J. A. Staps, and J. Beckers, "Characterization of cyclic dust growth in a low-pressure, radio-frequency driven argon-hexamethyldisiloxane plasma," *J. Phys. D: Appl. Phys.* **55**, 395203 (2022).
- ¹⁶S. Ratynskaia, A. Bortolon, and S. I. Krashennikov, "Dust and powder in fusion plasmas: Recent developments in theory, modeling, and experiments," *Rev. Mod. Plasma Phys.* **6**, 20 (2022).
- ¹⁷J. Beckers, T. van de Ven, R. van der Horst, D. Astakhov, and V. Banine, "EUV-induced plasma: A peculiar phenomenon of a modern lithographic technology," *Appl. Sci.* **9**, 2827 (2019).
- ¹⁸M. A. van de Kerkhof, T. van Empel, M. Lercel, C. Smeets, F. van de Wetering, A. Nikipelov, C. Cloin, A. Yakunin, and V. E. Banine, "Advanced particle contamination control in EUV scanners," *Proc. SPIE* **10957**, 109570U (2019).
- ¹⁹J. Beckers, B. van Minderhout, P. Blom, G. Kroesen, and T. Peijnenburg, "Particle contamination control by application of plasma," *Proc. SPIE* **11323**, 558–563 (2020).
- ²⁰P. Blom, J. C. A. van Huijstee, F. Medini, R. Baade, and J. Beckers, "Plasma-assisted removal of particles: Taming the beast," *Mikroniek* **6**, 15–18 (2021).
- ²¹M. A. Lieberman and A. J. Lichtenberg, *Principles of Plasma Discharges and Materials Processing*, 2nd ed. (John Wiley & Sons, 2005).
- ²²J. Beckers, R. Gopalakrishnan, and J. Goree, "Editorial: Particle interaction with afterglow plasma and non-quasi-neutral plasma," *Front. Phys.* **10**, 1–2 (2022).
- ²³L. Couëdel, "Temporal dusty plasma afterglow: A review," *Front. Phys.* **10**, 1–13 (2022).
- ²⁴T. J. A. Staps, "A review of nanoparticle decharging in atmospheric pressure plasma afterglows," *Front. Phys.* **10**, 988812 (2022).
- ²⁵L. Couëdel, A. Mezeghrane, A. A. Samarian, M. Mikikian, Y. Tessier, M. Cavarroc, and L. Boufendi, "Complex plasma afterglow," *Contrib. Plasma Phys.* **49**, 235–259 (2009).
- ²⁶I. B. Denysenko, M. Mikikian, and N. A. Azarenkov, "Modeling results on the dust charge distribution in a plasma afterglow," *Phys. Plasmas* **29**, 093702 (2022).
- ²⁷V. Suresh, L. Li, J. R. Go Felipe, and R. Gopalakrishnan, "Modeling nanoparticle charge distribution in the afterglow of non-thermal plasmas and comparison with measurements," *J. Phys. D: Appl. Phys.* **54**, 275205 (2021).
- ²⁸I. B. Denysenko, M. Mikikian, and N. A. Azarenkov, "Dust dynamics during the plasma afterglow," *J. Phys. D: Appl. Phys.* **55**, 095201 (2022).
- ²⁹N. Chaubey, J. Goree, S. J. Lanham, and M. J. Kushner, "Positive charging of grains in an afterglow plasma is enhanced by ions drifting in an electric field," *Phys. Plasmas* **28**, 103702 (2021).
- ³⁰V. Schneider, "Optisch gefangene mikropartikel als sonden in einem hochfrequenz-niederdruckplasma," Ph.D. thesis (Christian-Albrechts-Universität, 2020).
- ³¹L. Wörner, A. V. Ivlev, L. Couëdel, P. Huber, M. Schwabe, T. Hagl, M. Mikikian, L. Boufendi, A. Skvortsov, A. M. Lipaev, V. I. Molotkov, O. F. Petrov, V. E. Fortov, H. M. Thomas, and G. E. Morfill, "The effect of a direct current field on the microparticle charge in the plasma afterglow," *Phys. Plasmas* **20**, 123702 (2013).
- ³²X. Chen and C. J. Hogan, "Nanoparticle dynamics in the spatial afterglows of nonthermal plasma synthesis reactors," *Chem. Eng. J.* **411**, 128383 (2021).
- ³³E. Husmann, E. Thimsen, and X. Chen, "Particle charge distributions in the effluent of a flow-through atmospheric pressure low temperature plasma," *Plasma Sources Sci. Technol.* **30**, 075030 (2021).
- ³⁴N. Chaubey and J. Goree, "Preservation of a dust crystal as it falls in an afterglow plasma," *Front. Phys.* **10**, 1–9 (2022).
- ³⁵S. Dhawan, A. Vidwans, G. Sharma, N. H. Abuyazid, R. M. Sankaran, and P. Biswas, "Enhancing charging and capture efficiency of aerosol nanoparticles using an atmospheric-pressure, flow-through RF plasma with a downstream DC bias," *Aerosol Sci. Technol.* **54**, 1249–1254 (2020).
- ³⁶A. V. Ivlev, M. Kretschmer, M. Zuzic, G. E. Morfill, H. Rothermel, H. M. Thomas, V. E. Fortov, V. I. Molotkov, A. P. Nefedov, A. M. Lipaev, O. F. Petrov, Y. M. Baturin, A. I. Ivanov, and J. Goree, "Decharging of complex plasmas: First kinetic observations," *Phys. Rev. Lett.* **90**, 055003 (2003).
- ³⁷G. Sharma, N. Abuyazid, S. Dhawan, S. Kshirsagar, R. M. Sankaran, and P. Biswas, "Characterization of particle charging in low-temperature, atmospheric-pressure, flow-through plasmas," *J. Phys. D: Appl. Phys.* **53**, 245204 (2020).
- ³⁸B. van Minderhout, J. C. A. van Huijstee, A. T. A. Peijnenburg, P. Blom, G. M. W. Kroesen, and J. Beckers, "Charge neutralisation of microparticles by pulsing a low-pressure shielded spatial plasma afterglow," *Plasma Sources Sci. Technol.* **30**, 045016 (2021).
- ³⁹J. C. A. van Huijstee, P. Blom, A. T. A. Peijnenburg, and J. Beckers, "Spatio-temporal plasma afterglow induces additional neutral drag force on microparticles," *Front. Phys.* **10**, 926160 (2022).
- ⁴⁰B. van Minderhout, A. T. A. Peijnenburg, P. Blom, J. M. Vogels, G. M. W. Kroesen, and J. Beckers, "The charge of micro-particles in a low pressure spatial plasma afterglow," *J. Phys. D: Appl. Phys.* **52**, 32LT03 (2019).
- ⁴¹B. van Minderhout, J. C. A. van Huijstee, B. Platier, A. T. A. Peijnenburg, P. Blom, G. M. W. Kroesen, and J. Beckers, "Charge control of micro-particles in a shielded plasma afterglow," *Plasma Sources Sci. Technol.* **29**, 065005 (2020).
- ⁴²B. van Minderhout, J. C. A. van Huijstee, R. M. H. Rempelberg, A. Post, A. T. A. Peijnenburg, P. Blom, and J. Beckers, "Charge of clustered microparticles measured in spatial plasma afterglows follows the smallest enclosing sphere model," *Nat. Commun.* **12**, 4692 (2021).
- ⁴³B. van Minderhout, "Microparticle charging in spatial plasma afterglows," Ph.D. thesis (Eindhoven University of Technology, 2021).
- ⁴⁴W. Rogowski, "Die elektrische Festigkeit am Rande des Plattenkondensators - Ein Beitrag zur Theorie der Funkenstrecken und Durchführungen," *Arch. Elektrotech.* **12**, 1–15 (1923).
- ⁴⁵P. S. Epstein, "On the resistance experienced by spheres in their motion through gases," *Phys. Rev.* **23**, 710–733 (1924).
- ⁴⁶R. Limpens, B. Platier, A. C. Lassise, T. J. Staps, M. A. van Nijnhuijs, O. J. Luiten, and J. Beckers, "Influence of a magnetic field on an extreme ultraviolet photon-induced plasma afterglow," *J. Phys. D: Appl. Phys.* **54**, 435205 (2021).

- ⁴⁷W. Allis, "Motions of ions and electrons," in *Handbuch der Physik*, edited by S. Flügge (Springer-Verlag, Berlin, 1956).
- ⁴⁸A. V. Phelps, "Diffusion of charged particles in collisional plasmas. Free and ambipolar diffusion at low and moderate pressures," *J. Res. Natl. Inst. Stand. Technol.* **95**, 407–431 (1990).
- ⁴⁹W. P. Allis and D. J. Rose, "The transition from free to ambipolar diffusion," *Phys. Rev.* **93**, 84–93 (1954).
- ⁵⁰K. Katsonis, C. Berenguer, A. Kaminska, and M. Dudeck, "Argon 4s and 4p excited states atomic data applied in ARC-JET modeling," *Int. J. Aerosp. Eng.* **2011**, 896836.
- ⁵¹S. A. Khrapak, S. V. Ratynskaia, A. V. Zobnin, A. D. Usachev, V. V. Yaroshenko, M. H. Thoma, M. Kretschmer, H. Höfner, G. E. Morfill, O. F. Petrov, and V. E. Fortov, "Particle charge in the bulk of gas discharges," *Phys. Rev. E* **72**, 016406 (2005).